ACADEMIC PRESS

Available online at www.sciencedirect.com
SCIENCE DIRECT®

Journal of Catalysis 214 (2003) 261–272

JOURNAL OF CATALYSIS

www.elsevier.com/locate/jcat

# Redox interplay at copper oxide-(Ce, Zr)$O_x$ interfaces: influence of the presence of NO on the catalytic activity for CO oxidation over $CuO/CeZrO_4$

A. Martínez-Arias,[a,*] M. Fernández-García,[a] A.B. Hungría,[a] A. Iglesias-Juez,[a] O. Gálvez,[a,1] J.A. Anderson,[b] J.C. Conesa,[a] J. Soria,[a] and G. Munuera [c]

[a] *Instituto de Catálisis y Petroleoquímica, CSIC, C/ Marie Curie, Campus Cantoblanco, 28049 Madrid, Spain*
[b] *Division of Physical and Inorganic Chemistry, University of Dundee, Dundee, DD14HN Scotland, UK*
[c] *Departamento de Química Inorgánica, Universidad de Sevilla, 41092 Sevilla, Spain*

Received 6 August 2002; revised 21 October 2002; accepted 24 October 2002

**Abstract**

A catalyst composed of copper oxide supported on cerium–zirconium mixed oxide ($CuO_x/CeZrO_4$) has been studied with respect to its activity for CO oxidation under stoichiometric conditions employing either oxygen or oxygen with a small amount of NO as oxidant. The nature of copper oxide entities, as well as the redox properties of the catalyst following interactions with CO and $O_2$–NO, has been studied by XPS, EPR, and static NO adsorption infrared spectroscopy while in situ DRIFTS has been employed to follow processes occurring at the catalyst surface under reaction conditions. Characterization of the copper oxide species in both fully oxidized and partially reduced states reveals that they are significantly affected by interactions with the underlying support. On the basis of catalytic activity results and in combination with analysis of the evolution of particular $Cu^+$ carbonyls, comparing the CO oxidation reaction in the presence and absence of NO, it is proposed that the two basic factors affecting the catalytic performance of this type of system are the facility for achieving a partially reduced state for the copper oxide phase at the interfacial zone and the redox properties of the $CuO_x/CeZrO_4$ interface.


*Keywords:* Copper oxide; Ce–Zr mixed oxide; Ceria-based catalysts; CO oxidation; Nitric oxide; XPS; $Cu^{2+}$ EPR; NO adsorption infrared; In situ DRIFTS

## 1. Introduction

Catalysts based on ceria or cerium–zirconium mixed oxides present a wide range of applications, such as three-way catalysts for automobile exhaust gas emission control, removal of $SO_x$–$NO_x$ from fluid catalytic cracking flue gases, electrocatalysts over fuel cell electrodes, and catalysts for various oxidation and hydrogenation reactions [1–4]. For most of these applications, ceria–related compounds are thought to operate mainly as promoters of the active metal (or metal oxides) with which they are in contact [1]. Depending on the type of reaction and the experimental conditions involved in each case, different promoting effects including structural, redox states, and bifunctional promotions have been proposed to account for the synergetic effects observed [1].

One of the reactions in which the promoting effect is most significant is carbon monoxide oxidation. For this reaction, it is interesting that ceria-related oxides promote the activity of both noble metals (for instance, Rh, Pt, and/or Pd, typically present in TWC) and nonnoble metals or metal oxides [1,2,5–16]. Among the latter, outstanding activities, comparable to those exhibited by noble metal catalysts, are shown by copper catalysts [5–17]. Different hypotheses have been made to account for the synergetic effects on CO oxidation observed upon establishment of interactions between copper oxide and ceria–related oxides [5–17]. Concerning the nature of the active copper species, it is generally accepted that these are related to well-dispersed states of copper (having a small nuclearity and probably in the form of copper oxide clusters [16]) in contact with the ceria-based support [5–7,

* Corresponding author.
*E-mail address:* amartinez@icp.csic.es (A. Martínez-Arias).
[1] Present address: Departamento de Química-Física, Facultad de Química, Universidad Complutense, 28040 Madrid, Spain.

0021-9517/03/$ – see front matter 
doi:10.1016/S0021-9517(02)00084-2

9,11,14–17]. Correlation between the reducibility of highly dispersed copper oxide species and their catalytic activity appears to be well established [9,11,14–20]. Recent results have shown that these sites display a facile redox interplay with the reactants, suggesting that the reaction follows a redox mechanism [16]. Furthermore, the redox states of both catalyst components (copper and ceria-related oxides) appear to undergo concomitant changes, strongly suggesting that the active sites are located at the interfacial region [16], in agreement with previous postulations [5,7,14,17,19]. Differences between the activities of copper oxide catalysts supported on different ceria-based oxides have been related to the different redox activities of the $O^{2-}/V_{\ddot{O}}$ (where $V_{\ddot{O}}$ denotes a doubly ionized oxygen vacancy, using the Kröger–Vink notation) interface sites in each case [16]. A somewhat different mechanistic proposal has been recently put forward by Wang et al. [21]. In their approach, the reaction is proposed to take place in two general sets of processes covering an induction and a light-off period. Although a role for interface vacancies at the support is recognized, this role appears to be mainly restricted to facilitating oxygen activation during the induction steps prior to light-off, while sites responsible for light-off behavior are proposed to be related to oxygen vacancies at the copper oxide [21]. On the other hand, an important role of the surface structure of the ceria-related oxide in the copper oxide activity for the reaction has been proposed by Skårman et al. in a report showing significant differences between the activities of copper oxide thin films supported on $CeO_2${111} and $CeO_2${001} surfaces [22].

The present work aims to provide further insight into processes involved in the mechanism of CO oxidation in this kind of system by extending previous results obtained for the same reaction over a $CuO/CeZrO_4$ catalyst [16]. In this case, a small amount of NO (within a stoichiometric CO–$O_2$–NO mixture) has been included in the reactant stream in order to introduce a certain distortion into the CO oxidation processes. It should be noted that NO is able to compete with CO for oxidized copper sites and with oxygen for interfacial vacancies [23–25] and could therefore potentially affect the redox properties of both catalyst components and, as a consequence, the overall catalytic activity of the system. Preliminary catalytic activity results, for bimetallic Pd–Cu catalysts, have shown that NO has little influence on CO oxidation activity over the $CuO/CeZrO_4$ catalyst [26]. A more detailed study of the reasons underlying this behavior is presented here.

## 2. Experimental

### 2.1. Materials

A high-surface-area ($S_{BET} = 96\ m^2\ g^{-1}$) Zr–Ce (atomic ratio 1 : 1) mixed oxide was used as the support. It was prepared by a microemulsion–coprecipitation method by mixing two reverse microemulsions containing aqueous phases prepared by dissolving similar molar amounts of cerium (III) nitrate hexahydrate and zirconyl nitrate for the first and tetramethylammonium hydroxide pentahydrate for the second, dispersed in an organic solvent (*n*-heptane), using Triton X-100 (Aldrich) as surfactant and hexanol as co-surfactant. Following centrifugation, decanting, and rinsing of the resulting solid with methanol, it was dried at 383 K for 24 h and finally calcined in air at 773 K for 2 h. Further details on the preparation and characteristics of this support can be found elsewhere [27]. Thorough precipitation of both cerium and zirconium components was achieved for this support (on the basis of ICP-AES analysis of the final product); it consisted of ca. 5-nm crystallites (based on TEM results; XRD estimation of the particle size showed good agreement with the TEM observation) presenting the fluorite-related pseudocubic phase $t''$ (on the basis of XRD and Raman analyses) and showing reasonably good compositional homogeneity at the atomic scale [27].

A sample of copper catalyst supported on the $CeZrO_4$ mixed oxide (referred to hereafter as CuZC) was prepared by incipient wetness impregnation of the above support using an aqueous solution of $Cu(NO_3)_2 \cdot 3H_2O$ (to give a final copper loading of 1 wt%, representing ca. 157 μmol of Cu per gram of catalyst). The resulting material was dried overnight at 383 K and subsequently calcined in air at 773 K for 2 h. XRD and Raman analyses of the CuZC sample showed only features similar to those observed for the copper-free support.

All the gases employed were of commercial purity (CO: 99.9%; $O_2$: 99.99%; NO: 98.5%, with 1% $NO_2$ and 0.5% $N_2O$ as the main impurities) and, for experiments using the vacuum line (static IR and EPR experiments), were further purified by vacuum distillation before storage.

### 2.2. Techniques

Light-off catalytic activity tests were carried out using a glass flow reactor system loaded with ca. 3 g of sample. Catalyst particles in the range 0.125–0.250 mm were selected after pelleting, grinding, and sieving in order to minimize the pressure drop and internal diffusion effects, while the reactor geometry was optimized to avoid significant external diffusion effects [28]. Analysis of the feed and outlet gas streams was performed using a Perkin–Elmer FTIR spectrometer model 1725X, coupled to a multiple reflection transmission cell (Infrared Analysis Inc. long path gas minicell, path length 2.4 m, internal volume ca. 130 $cm^3$), the $O_2$ concentration in the gas stream was determined with a paramagnetic analyzer (Servomex 540 A). Prior to catalytic testing, the catalysts were subjected to a standard calcination pretreatment using 3% $O_2/N_2$ flow at 773 K for 1 h, cooled to room temperature (RT) in the same flow, and finally briefly purged in $N_2$. The catalytic tests were performed under stoichiometric conditions in 1% CO and 0.5% $O_2$ or 1% CO, 0.45% $O_2$, and 0.1% NO, using $N_2$ as carrier gas at atmospheric pressure, a fixed space velocity of

$3 \times 10^4$ $h^{-1}$ (roughly corresponding to 0.18 g s $cm^{-3}$), and temperature ramps of 5 K $min^{-1}$; it must be noted that analysis of the bypass flow shows that around 45 ppm of $NO_2$ is present at RT in the latter gas mixture under these experimental conditions, due to partial homogeneous $NO/NO_2$ equilibration. In all cases, the runs were commenced after an initial equilibration period of ca. 5 min in the reactant flow at RT.

Diffuse reflectance infrared Fourier transform spectra (DRIFTS) under reaction conditions were recorded using a Perkin–Elmer 1750 FTIR spectrometer equipped with an MCT detector. The spectra were taken at resolution 4 $cm^{-1}$ and 10 scans were accumulated for every spectrum. The DRIFTS cell (Harrick) was fitted with $CaF_2$ windows and a heating cartridge which allowed samples to be heated to 773 K. Samples of ca. 80 mg were calcined in situ (in a manner similar to that of the catalytic activity tests) and then cooled to RT before introducing the reaction mixture (passing through the catalyst bed) consisting of 1% CO and 0.5% $O_2$ or 1% CO, 0.45% $O_2$, and 0.1% NO in $N_2$, and using a total flow of ca. 80 $cm^3$ $min^{-1}$ and ramps of 5 K $min^{-1}$. A PC-controlled gas blender was used to monitor the composition of the inlet gases.

Transmission infrared spectra under static conditions were recorded at RT with a Nicolet 5ZDX FTIR spectrometer with a resolution of 4 $cm^{-1}$, 128 scans per spectrum, subtracting the gas phase contribution in all cases. Thin self-supporting disks (ca. 20 mg $cm^{-2}$) were prepared by pressing the powders at 2500 N $cm^{-2}$ and were handled in standard greaseless cells, where they could be subjected to thermal or adsorption treatments. The reduction treatments under CO were carried out under conditions similar to those indicated below for the EPR experiments.

Electron paramagnetic resonance (EPR) spectra were recorded at 77 K with a Bruker ER 200 D spectrometer operating in the X-band and calibrated with a DPPH standard ($g = 2.0036$). Portions of sample of about 30 mg were placed inside a quartz probe cell with greaseless stopcocks using a conventional high-vacuum line (capable of maintaining a dynamic vacuum of ca. $6 \times 10^{-3}$ N $m^{-2}$) for the different treatments. In all cases, the sample was pretreated in 300 Torr (1 Torr = 133 N $m^{-2}$) of pure oxygen at 773 K for 2 h. CO reduction treatments at a specific reduction temperature ($T_r$) were made under static conditions using 100 Torr of CO, heating for 1 h at the corresponding $T_r$ and subsequently outgassing at the same temperature for 0.5 h. Quantitative evaluation of the amount of species present in the spectra was performed by double integration of the corresponding EPR spectra and comparison with a copper sulfate standard.

X-ray photoelectron spectra (XPS) were recorded with a Leybold–Heraeus spectrometer equipped with an EA-200 hemispherical electron multichannel analyzer (from Specs) and a 120-W, 30-mA Mg-$K_\alpha$ X-ray source. A PC was used to control the instrument and recording of the spectra. The CuZC sample (0.2 g) was lightly pressed into a small ($4 \times 4$ $mm^2$) pellet and then mounted on a sample rod and introduced into the pretreatment chamber where it was outgassed at 473 K for 2–3 h, until a pressure of less than $2 \times 10^{-8}$ Torr was achieved, the sample then being reoxidized under 1 Torr of $O_2$ at the same temperature. Subsequently, it was reduced under 1 Torr CO at 373 K and then contacted with increasing doses of $10^{-4}$, $10^{-2}$, and 1 Torr of either $O_2$ or NO. Following each treatment, the sample was moved into the ion-pumped analysis chamber, where it was further outgassed until a pressure less than $2 \times 10^{-9}$ Torr was attained (2–3 h). This low pressure was maintained during all the data acquisition by ion pumping of the chamber. After each treatment, XP spectra in the relevant energy windows were collected for 20 to 90 min, depending on the peak intensities, at a pass energy of 44 eV (1 eV = $1.602 \times 10^{-19}$ J), which is typical of high-resolution conditions. The intensities were estimated by calculating the integral of each peak after subtraction of an S-shaped Shirley-type background with the help of UNIFIT for Windows (Version 3.2) software [29]; atomic ratios were then derived using the appropriate experimental sensitivity factors. All binding energies (BE) were referenced to the adventitious C 1*s* line at 284.6 eV. This reference gave BE values with an accuracy of ±0.1 eV; the peak $u'''$ characteristic of $Ce^{4+}$ was thus obtained at 917.0 ± 0.1 eV. In the case of Ce 3*d* spectra, factor analysis (FA) was used to calculate the $Ce^{3+}/Ce^{4+}$ ratios in each set of spectra recorded, using the methodology developed in a previous work [30].

## 3. Results

### 3.1. Catalytic activity tests

The results obtained for the CO–$O_2$ and CO–$O_2$–NO reactions are shown in Fig. 1. Mass balance analysis of the evolution of the different gas reactants and products present during the CO–$O_2$–NO reaction indicates that the NO conversion profile is affected by adsorption–desorption effects for $T \lesssim 450$ K; therefore, only conversion points above that temperature can be considered as representative of NO reduction with CO. Analysis of the various reactivity profiles shows that decomposition of adsorbed $NO_x$ species (below ca. 430 K) produces mainly NO and concomitantly a very small amount of $N_2O$, while NO reduction with CO (taking place at $T \gtrsim 450$ K) is essentially 100% selective to $N_2$. Interestingly, CO oxidation with $O_2$ (responsible for CO conversion at $T \lesssim 450$ K) is very slightly affected by the presence of NO in the reactant mixture. This contrasts with the behavior observed for noble metal catalysts promoted by ceria-related oxides for which, under conditions similar to those employed here, the activity of CO oxidation with $O_2$ is decreased by the presence of NO in the reactant mixture [26,31].

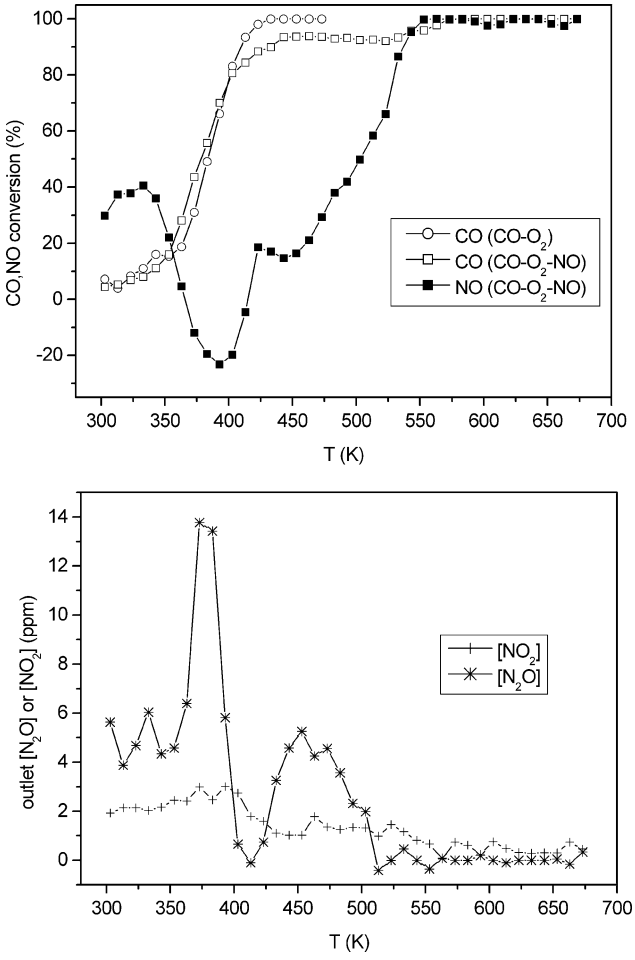


Fig. 1. Top: Conversion profiles obtained during the CO–$O_2$–NO and CO–$O_2$ reactions over CuZC. Bottom: Outlet $N_2O$ and $NO_2$ concentrations observed during the course of the CO–$O_2$–NO reaction.

### 3.2. Infrared results

DRIFT spectra recorded at increasing temperatures under CO–$O_2$–NO reaction conditions are shown in Fig. 2. A reasonable correlation is apparent between the evolution of gas phase CO and $CO_2$ (appearing as relatively broad bands at 2200–2050 and 2400–2300 $cm^{-1}$, respectively) and the catalytic activity results (Fig. 1). Unfortunately, the smaller extinction coefficient and concentration of NO(g) prevent its detection in the spectra under the conditions employed. Only one band in the range 2111–2105 $cm^{-1}$ appears under the reaction conditions in the carbonyl-stretching region of the spectra. This band is characteristic of carbonyl species adsorbed on copper sites in contact with ceria-related oxides and, although its frequency would appear somewhat low for a cationic copper site, it has been attributed to $Cu^+$ carbonyls on the basis of its relatively high thermal stability during outgassing [16,18,19]. The evolution of its intensity as a function of the reaction temperature in the presence and absence of NO in the reactant mixture is displayed in Fig. 3. Notably, significant differences are observed between the two experiments in the evolution of the band intensity, in spite of the close similarities observed for the CO–$O_2$ activity profiles (Fig. 1), and as confirmed by the simultaneous monitoring of the $CO_2$ gas phase bands during the in situ DRIFTS experiments (Fig. 3). A better degree of correlation is observed when catalytic activity and the $\nu$CO of the $Cu^+$ carbonyl are compared as functions of increasing reaction temperature (Fig. 3, bottom). In this respect, it is significant that the profiles in the presence of NO show a rough degree of correlation between the onset of CO oxidation and a small increase in the $Cu^+$ carbonyl intensity along with a sharper wavenumber decrease for that band. It is also clear that no

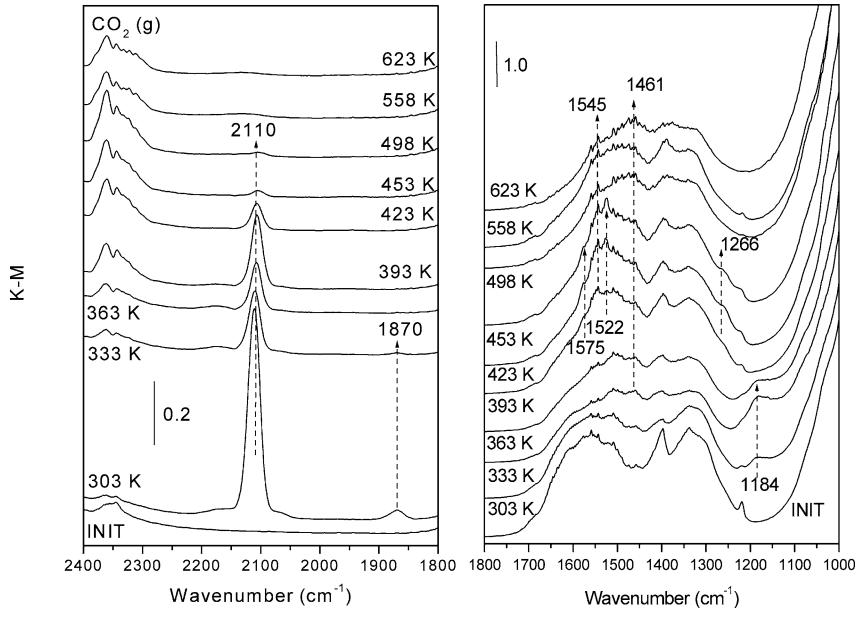


Fig. 2. In situ DRIFTS spectra observed during the course of the CO–$O_2$–NO reaction at the indicated temperatures. The label INIT refers to the spectrum recorded prior to introduction of the reaction mixture.

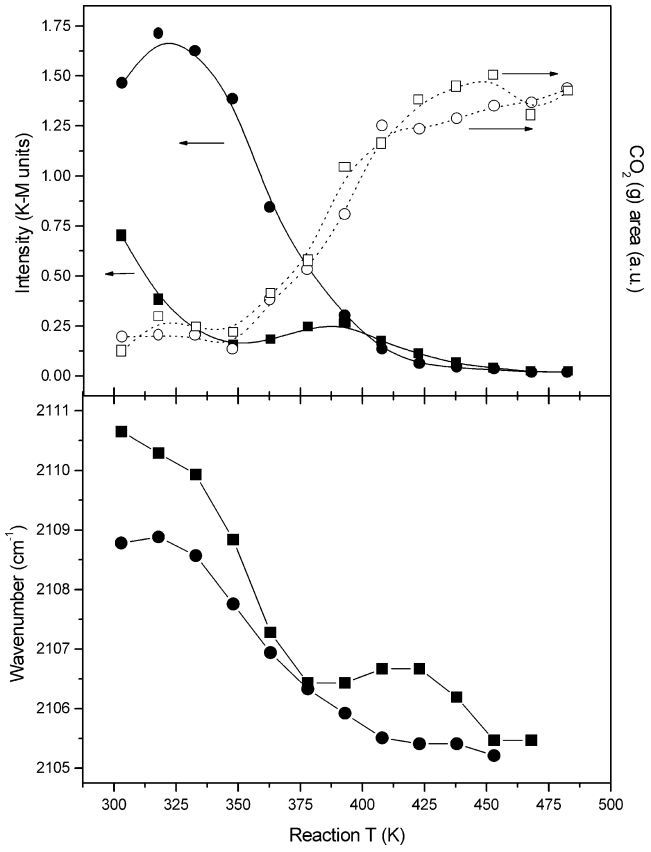


Fig. 3. Top: Intensities observed by DRIFTS for the $Cu^+$ carbonyl at 2111–2105 $cm^{-1}$ (solid lines) and the $CO_2$(g) bands (dotted lines) during the course of the CO–$O_2$ (circles) and CO–$O_2$–NO (squares) reactions. Bottom: Evolution of $\nu$CO for the $Cu^+$ carbonyl during CO–$O_2$ (circles) and CO–$O_2$–NO (squares) reactions.

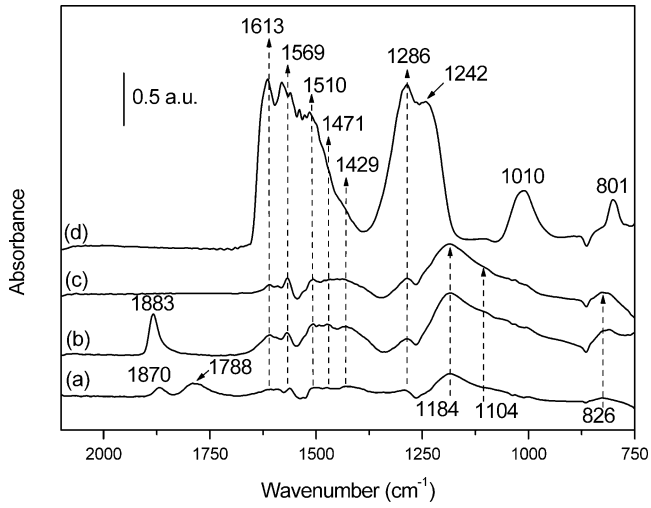


Fig. 4. Static infrared results observed for the CuZC sample reduced under CO at $T_r = 373$ K (the spectrum obtained after this treatment is taken as the reference for the difference spectra shown in the figure): (a) following exposure to 10 Torr of NO at RT; (b) subsequent exposure to 100 Torr of NO at RT; (c) subsequent outgassing at RT; (d) exposure to 10 Torr of NO + 45 Torr of $O_2$ at RT.

correlation exists between CO coverage (assuming it is proportional to band intensity) and the $Cu^+$ carbonyl stretching frequency (Fig. 3). This is further confirmed by examining the postreaction catalyst. For this purpose, the catalyst was cooled under $N_2$ at the end of the CO–$O_2$–NO reaction, and 1% CO was flowed over the catalyst at RT before flushing the cell with $N_2$ at RT and recording a spectrum under this inert atmosphere. Under these conditions (result not shown), the $Cu^+$ carbonyl band displayed an integrated intensity roughly four times larger than for the experiment conducted at 303 K under reaction conditions (Fig. 2) and shows a maximum at 2104 $cm^{-1}$.

Comparison with similar experiments performed in the absence of NO [16] enables one to determine the formation of bands derived from $NO_x$ adsorption or reaction. A band at 1870 $cm^{-1}$ appeared instantly upon contact with the CO–$O_2$–NO reactant mixture at 303 K and strongly decreased with increasing reaction temperature and was practically undetectable for $T > 363$ K. This band can be attributed to nitrosyl species adsorbed at exposed $Cu^{2+}$ cations [32]. Additionally, a band at 1184 $cm^{-1}$ also appeared upon contact with the reactant mixture at 303 K, reaching maximum intensity in spectra with the sample at 333 K and disappearing for $T \geqslant 393$ K. Other changes in the spectral range 1800–1000 $cm^{-1}$ which occurred during the course of the reaction are shown in Fig. 2, although complete resolution of the bands involved in these changes is difficult due to overlapping with bands already present for the initial sample, most likely due to bulk carbonate-type species, difficult to eliminate due to the relatively strong basic character of ceria-related materials [1]. It appears in any case that a band at 1461 $cm^{-1}$ evolves from 393 K while species giving rise to a set of bands and unresolved features at 1575, 1545, 1522, and 1266 $cm^{-1}$ are formed at intermediate temperatures (between 393 and 453 K).

Transmission infrared spectra following NO or NO + $O_2$ adsorption at RT on CuZC reduced under CO at 373 K are shown in Fig. 4. Exposure to 10 Torr of NO mainly generates species giving bands at 1870, 1788, and 1104 $cm^{-1}$, while weaker bands or shoulders are also apparent at 1613, 1569, 1510, 1471, 1429, 1286, 1104, and 826 $cm^{-1}$ (Fig. 4a). A subsequent increase in the NO pressure (up to 100 Torr) resulted in the disappearance of the band at 1788 $cm^{-1}$ and an increase of the rest of the bands with the maximum at 1870 $cm^{-1}$ being shifted to 1883 $cm^{-1}$ (Fig. 4b). The main modification produced upon subsequent outgassing at RT was the disappearance of the band at 1883 $cm^{-1}$ (Fig. 4c). On the other hand, strong bands and other unresolved features appeared upon exposure to NO + $O_2$, forming sets of overlapping bands in the ranges 1625–1400 and 1290–1240 $cm^{-1}$ with two weaker but well-defined bands at 1010 and 801 $cm^{-1}$.

Bands in the range 1900–1700 $cm^{-1}$ appearing upon NO adsorption are typical of adsorbed nitrosyl species, the difference between them being mainly related to the changes induced in the N–O bond resulting from changing the oxi-

dation state of the adsorption site [32]. Thus, bands at 1870 (or 1883) $cm^{-1}$, which are similar to those observed under CO–$O_2$–NO reaction conditions (Fig. 2), are assigned to nitrosyl species adsorbed on $Cu^{2+}$ cations, while the band at 1788 $cm^{-1}$ is assigned to nitrosyl species adsorbed on $Cu^{+}$ sites [32]. The band at 1184 $cm^{-1}$, which also appeared under reaction conditions (Fig. 2), is typical of chelating nitrite species coordinated to cerium cations [25]; its assignment to a species chemisorbed at sites on the support rather than at exposed copper oxide sites is supported by its observation on a $Pd/CeZrO_4$ sample treated under similar conditions [33]. The absorption at 1184 $cm^{-1}$ can be assigned to the $\nu_{asym}(NO_2)$ mode of the complex and the weaker band at 826 $cm^{-1}$ to the $\delta(NO_2)$ mode [25,32]; the $\nu_{sym}(NO_2)$ mode of the adsorbed complex, which is expected with a very weak intensity at ca. 1270 $cm^{-1}$ [25], is probably obscured by features corresponding to other species. The shoulder at 1104 $cm^{-1}$ is assigned to *trans*-hyponitrite species coordinated to cerium cations [25]. The series of bands at 1625–1400, 1290–1240, 1010, and 801 $cm^{-1}$ can be assigned to different adsorbed nitrate or nitro species [32,34–36].

### 3.3. EPR results

A previous report demonstrated in some detail the nature of $Cu^{2+}$ signals in CuZC in its initial calcined state as well as the evolution of the species as a function of treatments under CO at different reduction temperatures [16]. Approximately 38% of the entire copper content was detected for the initial calcined sample, the spectrum being mainly formed by a featureless broad signal showing extremes at $g = 2.21$ and $g = 2.04$, attributed to $Cu^{2+}$ cations in small copper oxide clusters, and a minor signal at $g_{||} = 2.233$ and $g_{\perp} = 2.036$ showing four-line hyperfine splittings in each of its components with $A_{||} = 16.0 \times 10^{-3}$ $cm^{-1}$ and $A_{\perp} = 1.8 \times 10^{-3}$ $cm^{-1}$, attributed to isolated $Cu^{2+}$ cations in a (generally speaking) tetragonally distorted octahedral symmetry. The portion of the copper which remained undetectable by EPR for the initial sample was proposed, on the basis of XPS results, to be due to magnetically coupled $Cu^{2+}$ species forming part of less dispersed copper oxide particles. A significant decrease in the $Cu^{2+}$ intensity, affecting both signals present in the spectrum, was produced upon reduction of the sample under CO at RT and 373 K. Thus, ca. 24 and 8% of the entire copper loading was detected as $Cu^{2+}$ after those experiments. Exposure of the reduced sample to oxygen at 77 K led to the appearance of superoxide species chemisorbed on cerium cations (formally $O_2^-$–$Ce^{4+}$ species) giving rise to signals at $g_z = 2.031$–$2.029$, $g_x = 2.016$, and $g_y = 2.011$ [16]. Formation of those species provided the principle evidence to indicate that support reduction had occurred, considering that paramagnetic $Ce^{3+}$ species are not easily detectable by EPR due to their short spin–lattice relaxation time [2].

On the basis of those results, a specific experimental protocol focused on determining the redox properties of CuZC upon interaction with $O_2$ or NO. For that purpose, a CuZC sample was prepared by reducing the initial calcined sample under CO at 373 K (followed by outgassing at the same temperature). Then, increasing amounts of either $O_2$ or NO were chemisorbed over that sample at RT, followed by thorough outgassing at the same temperature. The evolution of the $Cu^{2+}$ signals (identified mainly as $Cu^{2+}$ species within small copper oxide clusters) was then monitored during the reoxidation treatments. Following each of these treatments, the samples were exposed to $O_2$ (a dose of 70 µmol per g of catalyst) at 77 K (followed by outgassing at 77 K) and the evolution of $O_2^-$–$Ce^{4+}$ signals was monitored. The results obtained are shown in Fig. 5 and provide evidence that $O_2$ chemisorption induces a higher degree of copper oxidation than NO chemisorption and, in addition, the former is more effective in the elimination of centers which might form $O_2^-$–$Ce^{4+}$ species at 77 K.

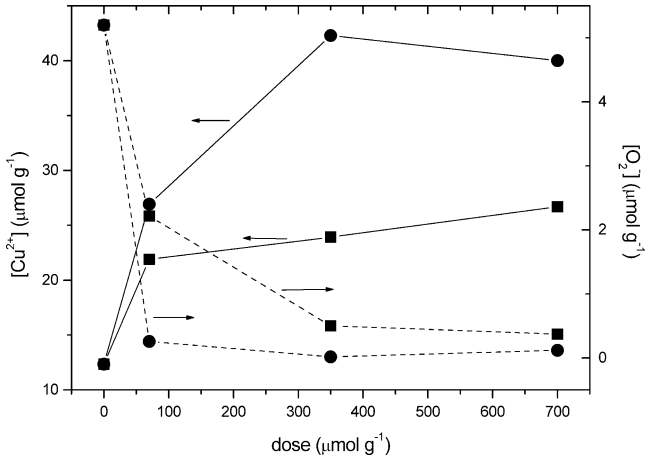


Fig. 5. Intensities of EPR signals due to $Cu^{2+}$ species (solid lines) and $Ce^{4+}$–$O_2^-$ species (dashed lines) as a function of the amount of $O_2$ (circles) or NO (squares) adsorbed at RT on CuZC reduced under CO at $T_r = 373$ K.

### 3.4. XPS results

No significant changes in the Cu/(Ce + Zr) and Ce/(Zr + Ce) atomic ratios were observed (Table 1) during the course of the treatments following a protocol very similar to that used for EPR experiments (see above). Values for those ratios were similar to those observed for the initial calcined sample or for the copper-free support, where a certain surface Ce enrichment was apparent [16,37]. These similarities indicate that the incorporation of the active copper phase does not modify the surface of the $CeZrO_4$ and that no significant changes in copper dispersion occur during the series of redox treatments.

Concerning changes in the redox state of cerium, the CuZC sample reduced in CO at 373 K contains ca. 15% $Ce^{3+}$, which is almost fully reoxidized (< 5% $Ce^{3+}$ remaining) immediately upon contact with $10^{-4}$ Torr of either $O_2$ or NO at RT. This provides further evidence for the presence of $Ce^{3+}$, as detected by EPR (through the formation of $Ce^{4+}$–$O_2^-$ species), after the reduction step. The pres-

ence of a small amount of $Ce^{3+}$ after the reoxidation experiments probably results from the effect of the ultra-high-vacuum environment removing the most labile chemisorbed oxygen species [16,25]. Certain changes were also observed in the Zr 3*d* signals during the course of the treatments. Thus, the relatively broad doublet observed for the sample reduced with CO at 373 K was narrowed upon contact with small amounts of NO, yielding a situation closer to that presented by the initial sample calcined at 773 K ($3d_{5/2}$ at $182.2 \pm 0.1$ eV and $3d_{3/2}$ $180.8 \pm 0.1$ eV). However, no significant modification of these signals was produced upon interaction with $O_2$. The broadening of the Zr 3*d* peaks can be tentatively interpreted as due to the high relative heterogeneity in the $Zr^{4+}$ coordination environments for the sample reduced by CO at 373 K rather than to changes in its oxidation state under such mild reduction conditions. The broader and slightly asymmetric Zr 3*d* doublet probably corresponds to a deconvolution of spectra and can be reasonably fitted using the same single set of parameters employed for the initial calcined sample, although larger FWHM values must be employed.

To examine in detail changes in the active Cu phase after each redox treatment, the energies of the Cu $2p_{3/2}$ and Cu($L_3M_{45}M_{45}$, $^1G$) peaks in Table 1 were plotted (Fig. 6), together with the modified Auger parameter ($\alpha' = E_B + E_K$), as Wagner-type chemical state diagrams. According to Wagner [38], the shifts in modified Auger parameter ($\alpha' = E_B + E_K$), which can be accurately measured in the presence of static sample charging and shown as lines of slope $-1$ in the diagrams, can be related to differences in the extraatomic relaxation energy ($\Delta\alpha' = 2\Delta R^{ea}$) for the core photohole according to a nonlocal screening mechanism (final state effects). On the other hand, within Moretti's electrostatic model [39], which assumes a nonlocal core-hole screening relaxation mechanism, the lines of slope $-3$ in these diagrams correspond to species with the same chemical state (i.e., similar initial state effects).

From the Wagner's plot in Fig. 6, it may be concluded that Cu in the initially CO-reduced CuZC catalyst is chemically similar to $Cu^+$ in bulk $Cu_2O$. However, the shift toward a lower value of $\alpha'$ within the dashed line of slope $-3$ crossing through the point for bulk $Cu_2O$ indicates a much smaller extraatomic relaxation of the photohole, according to the $\Delta\alpha = 2\Delta R^{ea}$ relationship. This suggests a strong contribution of the $CeZrO_4$ interface to the relaxation process, as previously reported by Mejias et al. for ultrathin $TiO_2$ films on different types of supports [40]. On the other hand, according to its position (Fig. 6), highly dispersed $Cu^+$ ions in Cu-exchanged Y-zeolites would experience a much lower core-hole extraatomic relaxation that can be related to the smaller polarizability of the oxide ions within the zeolitic framework than of oxide ions in bulk $Cu_2O$ [39,41]. Thus, we may conclude, in agreement with the EPR data above, that after reduction with CO at 373 K the active phase in CuZC is mostly reduced to a $Cu_2O$-like state, probably forming thin two-dimensional patches or small oxide clusters tightly interacting with the surface of the $CeZrO_4$support, in such a way that the less polarizable (in comparison with bulk compounds) oxide ions at this interface actively participate in the $Cu^+$ core-hole relaxation process.

Table 1 shows data for $E_B$ and $E_K$ obtained following reoxidation of the CO-reduced sample by either $O_2$ or NO, following a similar protocol to that employed for the EPR experiments. As observed in Fig. 6, increasing doses of $O_2$ at RT produce displacements in the Wagner chemical state diagram which, after a treatment with 1 Torr of $O_2$ at 473 K, reach a position that fits on the line of slope $-3$ corresponding to CuO. This suggests that $Cu^+$ cations in the $Cu_2O$-like phase are being progressively oxidized to $Cu^{2+}$, a process that is limited to ca. 40–45% after 1 Torr $O_2$ exposure at RT but reaches 100% at 473 K. This is supported by analysis of the $E_B$ and $E_K$ values for the intermediate oxidation steps, which correspond to deconvoluted spectra that include $Cu^+/Cu^{2+}$ components in the appropriate ratios. Two points are worthy of note here; first, a further reduction with CO at 373 K completely restores the original $E_B$ and $E_K$ values corresponding to $Cu_2O$-like patches with the same contribution of the support to the core photohole relaxation process; and second, according to the $E_B$ and $E_K$ values obtained for the sample reoxidized in 1 Torr of $O_2$ at 473 K, a quite similar effect of the interaction with the support on the relaxation process seems to occur in the fully oxidized CuO-like state. This suggests that the copper dispersion is roughly maintained throughout the series of treatments, since copper agglomeration and growth to give

Table 1
XPS data of CuZC reduced under CO at 373 K and subsequently reoxidized with $O_2$ or NO at RT

| Treatment | Cu/(Ce + Zr) | Ce/(Ce + Zr) | O/(Ce + Zr) | Cu 2*p* $E_B$ (eV) | Cu (AES) $E_K$ (eV) | $\alpha'$ (Cu) (eV) |
|---|---|---|---|---|---|---|
| CO/1 Torr/373 K | 0.076 | 0.59 | 2.00 | 932.8 | 915.3 | 1848.1 |
| $O_2/10^{-4}$ Torr/RT | 0.064 | 0.59 | 1.98 | 933.1 | 915.7 | 1848.6 |
| $O_2/10^{-2}$ Torr/RT | 0.077 | 0.59 | 2.07 | 933.1 | 915.6 | 1848.7 |
| $O_2$/1 Torr/RT | 0.082 | 0.59 | 2.06 | 933.3 | 916.0 | 1849.3 |
| CO/1 Torr/373 K | 0.079 | 0.59 | 2.00 | 933.0 | 915.2 | 1848.2 |
| $NO/10^{-4}$ Torr/RT | 0.070 | 0.58 | 2.08 | 932.9 | 915.3 | 1848.2 |
| $NO/10^{-2}$ Torr/RT | 0.072 | 0.59 | 2.02 | 933.0 | 915.6 | 1848.6 |
| NO/1 Torr/RT | 0.081 | 0.59 | 2.17 | 933.2 | 915.6 | 1848.8 |

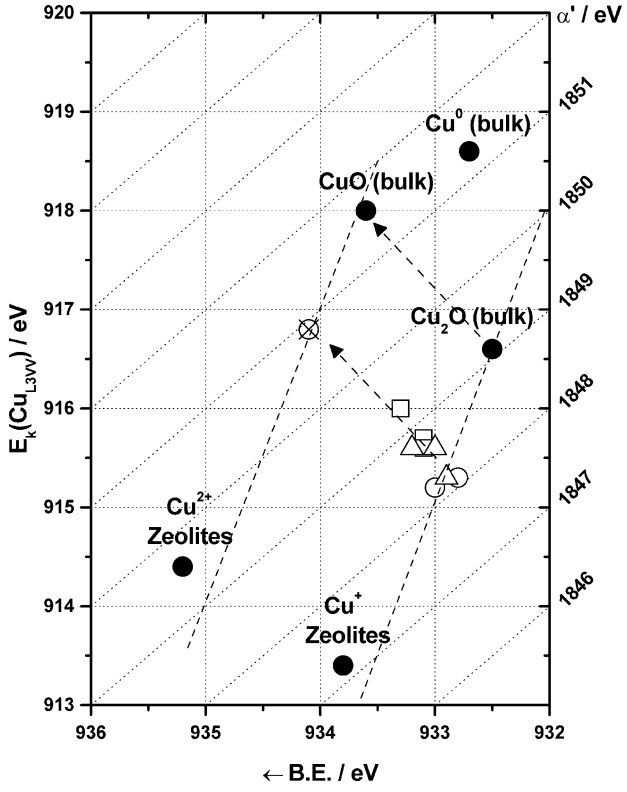


Fig. 6. Wagner diagram showing the evolution of Cu ($2p$ and AES) XPS parameters during reoxidation of CuZC reduced under CO at $T_r = 373$ K (open circles) with increasing amounts of either $O_2$ (open squares) or NO (open triangles). Parameters obtained for the sample reoxidized under 1 Torr of $O_2$ at 473 K are also shown (as a crossed circle point). Dashed lines of slope $-3$ are shown as a reference guide. Values for the reference samples (full circles) can be found elsewhere [39,41].

3D particles, either in a reduced or oxidized state, would produce a loss of the interaction with the $CeZrO_4$ surface and an increase in the contribution of oxide ions from bulk-like phases that would lead to displacements toward the $Cu_2O$ or CuO reference values shown in the diagram.

A gradual reoxidation from $Cu^+$ to $Cu^{2+}$ is also produced following interaction of the CO-reduced sample with increasing amounts of NO at RT. However, a lesser degree of oxidation (ca. 20–25% of $Cu^{2+}$), is achieved, compared with reoxidation under $O_2$, upon contact with 1 Torr of NO. Furthermore, the degree of oxidation only increases up to ca. 50% under heating at 473 K under 1 Torr of NO. Additionally, the concomitant growth of a small, very broad N 1$s$ signal, centered at 403.5 eV, is observed during the course of these experiments. This indicates the formation of tightly chemisorbed $NO_x$ species (not necessarily only on the $Cu_2O$ phase), in agreement with infrared results. In summary, and as previously found by EPR (Fig. 5), XPS data confirm that $O_2$ is a stronger oxidant than NO, either at RT or 473 K, for the reduced active Cu-phase in our CuZC catalyst. In addition, the strong interaction between the active copper component and the support is retained under the mild experimental conditions ($T < 473$ K). On the other hand, the small doses of both $O_2$ and NO are able to oxidize the reduced surface of the $CeZrO_4$ at RT, as shown by the observed evolution of the Ce 3$d$ XP spectra during the course of the treatments.

## 4. Discussion

Our previous report dealing with the CO oxidation reaction (employing $O_2$ alone as oxidant) over the CuZC catalyst proposed that the reaction follows a redox mechanism (of the Mars–van Krevelen type) in which the catalyst oscillates between an initial fully oxidized state (that may be represented as $Cu^{2+}$–$O^{2-}$–$Ce^{4+}$, taking into account the interface character of the active sites and considering formal charges for the sake of simplicity) and a partially reduced state ($Cu^+$–$V_{Ö}$–$Ce^{3+}$) [16]. This proposal was mainly based on the following experimental evidence [16].

(i) Reduction or oxidation of the catalyst is readily achieved upon interaction at low temperature with CO or $O_2$, respectively. In fact, these redox processes take place in CuZC even at RT, as indicated by in situ DRIFTS, EPR, CO-TPD results, and XPS. This contrasts with the greater difficulties encountered in trying to carry out similar redox processes over either pure $CuO_x$ or the Cu-free ceria-related oxide support [9,21,42], thus indicating the involvement in these redox processes of relatively strong synergetic interactions between both catalyst components. Involvement of the $Cu^{2+}$–$Cu^+$ redox pair instead of other alternatives (e.g., $Cu^{2+}$–$Cu^0$ or $Cu^+$–$Cu^0$ [21]) was mainly based on the absence of spectroscopic evidence of the formation of the $Cu^0$ state under reaction conditions, along with the relative ease with which the initial $Cu^{2+}$ state was restored upon interaction of the reduced catalyst with $O_2$, which is confirmed here by the XPS data analysis. Evidence for the presence of $Cu^{2+}$ states for the initial calcined CuZC catalyst was obtained by XPS and agrees with other XPS or EXAFS experiments performed on samples similar to the CuZC [15,42].

(ii) Regarding the nature of active sites, and in accordance with proposals by other authors [5,9,17], the interface sites between the copper oxide and the support were invoked in the reaction mechanism. This follows from the fact that the formation of $Cu^+$ carbonyl species (as characterized by DRIFTS) giving a band at ca. 2110 $cm^{-1}$ was observed under reaction conditions. As mentioned above, assignment of this band to $Cu^+$ carbonyl species, although at a position typical of $Cu^0$ carbonyls [43], was based on the relatively high stability of those carbonyl species during outgassing [16], in contrast to the typical behavior expected for $Cu^0$ carbonyls [19,44]. Indeed, the relatively low wavenumber observed for such particular carbonyls, in comparison with other $Cu^+$–CO species, was attributed to an interaction with the basic support [16,18,19,45], thus indicating that the species were formed on copper sites affected by an interaction with the ceria-related support [12,18,19]. Both the oxidation state of the copper adsorption centers responsible for

these carbonyls and its ascription to centers interacting with the support are supported by the XPS results here, as indicated by the analysis performed above. EPR results, on the other hand, showed the formation of $O_2^-$–$Ce^{4+}$ complexes upon oxygen chemisorption at 77 K on a mildly reduced CuZC sample ($T_r$ = RT) [16], in contrast to results observed for the support alone [19,46]. Such complexes were almost completely absent in CuZC after warming to RT. This was demonstrated to be due to the particular ease by which oxygen reduction occurred over the reduced surface (leading to diamagnetic species such as peroxide or oxide anions, whose formation requires the transfer of two or more electrons), which can be related to the high density of electrons (in the form of reduced cerium centers of the support) that become concentrated at the interface zone following reduction.

Furthermore, among the various kinds of $Cu^{2+}$ entities present in the catalysts (in the form of isolated cations, small CuO-type patches or clusters, or less dispersed copper oxide particles), it was proposed, mainly on the basis of their higher redox activity, that the active sites for the reaction were those involving contact between small CuO-type clusters and the ceria-related support [16]. This agrees with other proposals in the literature, which suggest that the copper-related active centers are associated with the finely dispersed states of copper oxide, which are able to maximize the number of $CuO_x$-support interface sites [5,11,17]. In this respect, it may be noted that isolated $Cu^{2+}$ species also show significant redox activity toward CO–$O_2$ [16,19], although they were disregarded as being the main source of catalytic activity in CuZC or similar catalysts, as they usually represent only a very small portion of the whole copper content of the catalyst [16].

To the best of our knowledge, little is known about the structural/morphological aspects of the active CuO-type clusters. The above description of the active phase of copper in terms of such copper oxide aggregates is mainly based on the fact that, in contrast with other supports such as alumina [47], no specific compounds appear to be formed between ceria-type and copper oxides, although some degree of solubility of oxidized copper in ceria seems possible in view of the changes in the fluorite lattice constant observed for this type of system [48]. Indeed, previous XPS results have revealed that the stabilization of most of the copper in this kind of catalyst is in the form of CuO-type phases [19]. From the EPR prospective, $Cu^{2+}$ cations within those CuO-type clusters, in addition to displaying significant redox activity (Fig. 5 and [16]), are characterized by a relatively broad signal without a clearly defined hyperfine structure in any of its components [16]. This is attributed to the presence of magnetic interactions between the $Cu^{2+}$ cations within the clusters, of a magnitude not sufficiently large to form antiferromagnetic couplings, which dominate in the case of well-formed CuO crystals [49]. Those spectral characteristics are also compatible with the presence of amorphous copper oxide layers with a disordered structure, which are considered to be the most active phase in the work by Harrison et al. [15]. It is interesting to note that in that study an important improvement in the parameter refinement was reported to be produced when a cerium atom at a distance of ca. 4.2 Å was included in the EXAFS analysis for that phase [15]. This suggests that the most active copper species can be related either to some kind of copper–cerium mixed oxide structure at a local level (as proposed for other systems of this kind [15,50,51]) or to thin two-dimensional raft-like copper oxide layers (2D patches), in which the properties of the $Cu^{2+}$ cations would differ from those in pure CuO as a consequence of their interaction with the underlying ceria-related support. This is supported by XPS analysis (Fig. 6), which indicates that most of the CuO in the CuZC catalyst is present as a highly dispersed thin phase in close interaction with the $CeZrO_4$ surface, so that the local electronic properties of the $Cu^{2+}$ ions (including the core-hole relaxation process) are greatly modified when compared with those of bulk CuO (or $Cu_2O$). A similar scenario has been envisaged for $Cu/TiO_2$ catalysts on the basis of IR spectroscopic evidence [52]. This modification induced by the support interaction can facilitate the $Cu^{2+}/Cu^+$ redox exchange conditions and the stabilization of adsorbed CO on the $Cu^+$ ions, which are readily formed even under stoichiometric CO + $O_2$ or CO + $O_2$ + NO mixtures.

Analysis of the evolution of the $Cu^+$ carbonyls giving the band at 2111–2105 $cm^{-1}$ under reaction conditions reveals interesting differences depending on the presence/absence of NO in the reaction mixture (Fig. 3). First, it can be considered that the intensity of this band is, in principle, a function of three different factors: the availability of $Cu^+$ sites at the sample surface (in contact with the ceria-related support, as discussed above); the concentration of CO in the reactant gas phase, which is a function of the extent of reaction; and the reaction temperature, which affects the adsorption/desorption equilibrium. Concerning the latter, the significant resistance of those carbonyls to desorption should be noted, since for CuZC significant intensity is still observed after RT CO adsorption on a (CO–$O_2$) post-reaction sample followed by extensive treatment from RT to 373 K under an inert gas flow [16]. Thus, taking the above factors into account and assuming that copper appears in a $Cu^{2+}$ state before interaction with the reaction mixture (as supported by XPS results), it appears reasonable that the initial low-temperature increase in band intensity under CO–$O_2$ is due to copper reduction under the stoichiometric reaction atmosphere. Taking into account that the evolution of the CO concentration must be similar for both reactions (considering the similar CO oxidation activities), the suppressed formation of the copper site giving this band in the presence of NO must, in principle, be related to either one of the other two factors or both, i.e., an NO-induced suppression of copper reduction to $Cu^+$ or a blocking effect of surface copper cations by $NO_x$-derived adsorbed species. Analysis of the NO-derived bands for the in situ DRIFTS spectra in Fig. 2

does not allow a definitive conclusion to be drawn in this respect. Only two bands of this kind are clearly observed at reaction temperatures that might be related to species that might affect the CO oxidation activity or the NO-induced suppression of $Cu^+$-carbonyl formation. In the first place, the $Cu^{2+}$ nitrosyl giving the band at 1870 $cm^{-1}$ does not appear to be responsible for the mentioned effects, on the basis of the mismatch between the evolution of the intensities of the respective bands (Fig. 2), since both the nitrosyl and the carbonyl show maximum intensity at 303 K and decrease at higher reaction temperatures. Second, the chelating nitrite species give the band at 1184 $cm^{-1}$. This, however, corresponds to a species adsorbed on the support and could only affect copper sites indirectly. Nevertheless, as shown in more detail in a previous study [25], those species are proposed to be formed by the interaction of NO with $Ce^{4+}$ sites most likely formed during support dehydroxylation (observed by in situ DRIFTS). Therefore, their formation would not in principle be affected by $CuO_x \rightarrow CeZrO_4$ electron transfer processes that could eventually lead to a higher degree of oxidation of the copper oxide phase. Those electron transfer processes would generate $Ce^{3+}$–$V_{\ddot{O}}$ sites, and these are not involved in the formation of the chelating nitrite [25], thus making it unlikely that formation of these species is involved to any extent in the NO-induced suppression of the copper oxide reduction process. In any case, it may be noted that the evolution of both NO-derived species (Fig. 2), but mainly that of the chelating nitrite species, accounts for the $NO_x$ adsorption/desorption phenomena observed at low reaction temperatures ($\lesssim$ 430 K) in the activity profiles (Fig. 1). Regarding the effects of other NO-derived species on the $Cu^+$-carbonyl formation, this is more difficult to resolve, due to the overlapping of several different bands in the corresponding spectral region. Therefore, it is not clear whether a blocking of $CuO_x$ sites by nitrate or nitro species is taking place, although bands corresponding to these species appear at relatively high temperatures and would not therefore affect CO oxidation activity or NO-induced suppression of $Cu^+$-carbonyl formation to any great extent. It would appear that the lower $Cu^+$-carbonyl intensity achieved in the presence of NO must be mainly related to the maintenance of a higher degree of oxidation at the copper oxide surface. This is supported by the comparatively higher wavenumber observed for the $Cu^+$ carbonyl when NO is present in the reaction mixture (Fig. 3) since, according to infrared studies of reduced copper oxide samples [18,44,53], the vibrational frequency of $Cu^+$ carbonyls decreases by increasing the degree of reduction around the $Cu^+$ adsorption center. This hypothesis is supported by the fact that the lower wavenumber for that band (2104 $cm^{-1}$) is observed in the post-reaction experiment where a maximum overall degree of reduction has been achieved on the basis of observation of the greatest intensity for the band under that condition. A question arises as to the reason that a higher overall degree of oxidation at the copper oxide phase (at least at low temperatures, before or immediately after $CO–O_2$ reaction onset) is achieved under stoichiometric $CO–O_2–NO$ than under stoichiometric $CO–O_2$. This is apparently in contradiction with EPR and XPS results (Figs. 5 and 6). While both NO and $O_2$ show a large capability to oxidize the reduced copper oxide phase (as also inferred from the evolution of the copper-related nitrosyls in the static infrared experiments of Fig. 4), the results clearly show the higher oxidizing power of $O_2$ than NO under the static equilibrium conditions employed. Experiments are under way to try to elucidate this phenomenon and two hypotheses are currently being considered: first, the effects of synergetic $NO–O_2$ interactions; second, the existence of a prevailing kinetic control governing the interactions of the different reactants under the dynamic conditions employed for the in situ DRIFTS or the catalytic tests.

The decrease in wavenumber of the $Cu^+$ carbonyl observed just prior to the onset of the $CO–O_2$ reaction (Fig. 3) suggests that the reaction is triggered as soon as a certain degree of reduction is achieved at the copper oxide phase. This resembles somewhat the processes which are proposed during the so-called "induction period," which precede catalyst light-off, in the reaction model proposed by Wang et al. [21]. However, in contrast to that model, the different intensities of the $Cu^+$ carbonyl observed in the presence or absence of NO just before reaction onset suggests that the location of the active sites for CO oxidation is largely restricted to a limited region of the catalyst, i.e., to copper oxide–$CeZrO_4$ interface positions, and that the reaction is not significantly extended onto copper oxide sites far beyond that region. A plausible model to account for the results obtained is depicted schematically in Fig. 7. Active sites are basically restricted to positions at the interface between the thin $CuO_x$ 2D-patches or more or less flat copper oxide layers (in order to account for the existence of relatively strong interactions between them and the underlying $(Ce, Zr)O_x$ support, according to XPS, infrared, and EPR results). Concerning processes occurring on the copper oxide phase, the presence of NO would mainly affect sites on the $CuO_x$ layer at positions relatively far from the active interface boundaries, restricting formation of $Cu^+$ carbonyls at those sites either through a blocking effect (by chemisorbed species) or by an oxidative interaction which favors the establishment of a higher degree of oxidation at these sites. On the basis of the absence of NO effects on the CO oxidation catalytic activity, it appears that NO does not strongly interact with the active interface sites and that the interactions with CO and oxygen prevail in that zone. It can be assumed that both the copper oxide and the support components of the interface are involved to some extent in the reaction mechanism by providing sites for activation of CO and $O_2$. In this way, the absence of NO competition with CO at the copper oxide component of the interface can be related with the attainment at a local level of a relatively high degree of reduction in that

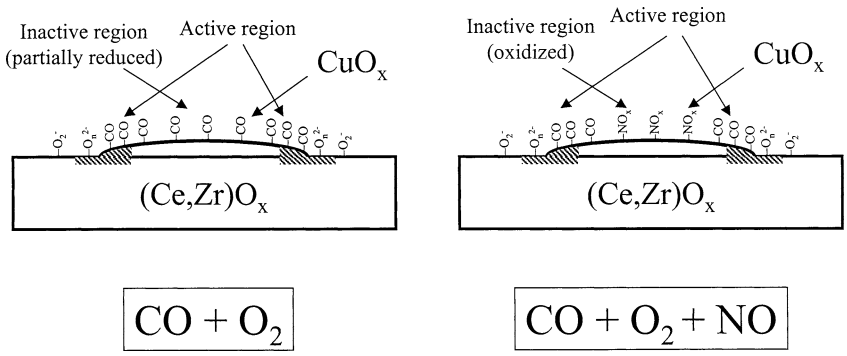


Fig. 7. Schematic model of the proposed active surface for the CuZC catalyst during the course of the CO–$O_2$ and CO–$O_2$–NO reactions.

zone (in agreement with analysis of the results of Fig. 3), if it is taken into account that CO predominantly interacts with reduced copper sites (and NO with oxidized sites) during CO–NO competition [23]. On the other hand, the prevailing interaction of oxygen, with respect to NO, with the active $Ce^{3+}$–$V_{Ö}$ interface sites at the support is demonstrated by the EPR results (Fig. 5). Thus, the largest hindrance to $O_2^-$–$Ce^{4+}$ formation produced when oxygen, in comparison with NO, is preadsorbed at RT reveals that oxygen is a more powerful oxidant than NO for the reduced active support sites.

Concerning other mechanistic aspects, the fact that the CO–$O_2$ catalytic activity appears to be restricted to the interface positions of the catalyst along with observation that a certain reductive preactivation of the copper oxide phase appears to be produced prior to the onset of reaction suggests that processes involved in the reaction mechanism for this kind of system must essentially depend on the properties of the interface between the partially reduced copper oxide entities and the ceria-based support. Two factors stand out as being most important in accounting for the catalytic properties for carbon monoxide oxidation in this kind of system. Both essentially depend on the characteristics of the copper oxide–ceria-based support synergetic interactions, although some specific properties of the individual components may also play a certain role. First, the facility for achieving partial reduction of the copper oxide entities at the interface zone, which, according to previous studies [6,9,21], is favored by an increase in dispersion of this component may be most significant in accounting for the different activities as a function of the level of copper oxide dispersion [6,9, 21]. In the second place, the redox properties of the interface sites between partially reduced copper oxide and the ceria-based support, which probably depends to some extent on the individual redox properties of the ceria-based support (for instance, the degree of unsaturation of the oxygen vacancy defects that can be generated, its surface acid/base properties, its electronic characteristics, etc.), may be the most important factor in explaining differences in the catalytic activities when the nature of the ceria-based support is varied [16].

## 5. Conclusions

The presence of copper oxide entities, most likely forming 2D patches or thin raft-like layers and strongly interacting with the $CeZrO_4$ support, is inferred from analysis of the Wagner diagram of the XPS results, both for the fully oxidized ($Cu^{2+}$) and partially reduced ($Cu^+$, achievable upon reduction under CO at 373 K) states of the catalyst, in agreement with analysis of $Cu^{2+}$ signals by EPR and of $Cu^+$ carbonyl infrared bands.

The behavior of the $CuO_x/CeZrO_4$ catalyst reduced under CO at 373 K toward reoxidation by either $O_2$ or NO has been examined by XPS and EPR. Both molecules readily oxidize both catalyst components, although oxygen displays the greater oxidizing power for both sites at the $CuO_x$ or (to a greater extent) $CeZrO_4$ parts of the catalyst.

No significant modifications were observed in the catalytic activity for CO oxidation (with oxygen) when NO is introduced (in a relatively small amount) into the stoichiometric reactant mixture. Analysis of this observation with the most important differences observed by in situ DRIFTS with respect to the intensity of $Cu^+$ carbonyls (at sites interacting with the $CeZrO_4$ support) in the presence and absence of NO suggest that the active zones of the catalyst for CO oxidation are largely restricted to the interface region. In turn, the evolution observed in the wavenumber of the $Cu^+$ carbonyls under reaction conditions suggests that the copper oxide component is reductively preactivated prior to the onset of CO oxidation. In general terms, the results obtained suggest that the two main factors governing the catalytic activity of this kind of system are the facility for partial prereduction of the copper oxide component at the interface zone (favored upon decreasing copper oxide particle size, although the role of the support as a redox promoter must also be considered) and the redox properties of the interface between that partially reduced copper oxide component and the underlying ceria-based support (specifically related to the characteristics of the $CuO_x$–support contacts and therefore strongly dependent on the support nature, i.e., the presence/absence of zirconium or other dopants in its composition).

## Acknowledgments

A.M.-A., A.B.H., and A.I.-J. thank the Comunidad de Madrid for grants received, under which this work was conducted, and for financial assistance (to A.M.-A.) under the program "Ayudas para estancias breves en centros de investigación extranjeros." Financial help by CICYT (Project MAT2000-1467) is also acknowledged.

## References

[1] A. Trovarelli, Catal. Rev. Sci. Eng. 38 (1996) 439.
[2] A. Trovarelli (Ed.), Catalysis by Ceria and Related Materials, in: Catalytic Science Series, Vol. 2, Imperial College Press, London, 2002.
[3] E.P. Murray, T. Tsai, S.A. Barnett, Nature 400 (1999) 649.
[4] S. Park, J.M. Vohs, R.J. Gorte, Nature 404 (2000) 265.
[5] W. Liu, A.F. Sarofim, M. Flytzani-Stephanopoulos, Chem. Eng. Sci. 49 (1994) 4871.
[6] W. Liu, M. Flytzani-Stephanopoulos, J. Catal. 153 (1995) 304.
[7] W. Liu, M. Flytzani-Stephanopoulos, J. Catal. 153 (1995) 317.
[8] A. Tschöpe, W. Liu, M. Flytzani-Stephanopoulos, J.Y. Ying, J. Catal. 157 (1995) 42.
[9] M.-F. Luo, Y.-J. Zhong, X.-X. Yuan, X.-M. Zheng, Appl. Catal. A 162 (1997) 121.
[10] P.W. Park, J.S. Ledford, Catal. Lett. 50 (1998) 41.
[11] M.-F. Luo, X.-M. Zheng, Acta Chem. Scand. 52 (1998) 1183.
[12] A. Martínez-Arias, J. Soria, R. Cataluña, J.C. Conesa, V. Cortés Corberán, Stud. Surf. Sci. Catal. 116 (1998) 591.
[13] P. Bera, S.T. Aruna, K.C. Patil, M.S. Hegde, J. Catal. 186 (1999) 36.
[14] J.B. Wang, W.-H. Shih, T.-J. Huang, Appl. Catal. A 203 (2000) 191.
[15] P.G. Harrison, I.K. Ball, W. Azelee, W. Daniell, D. Goldfarb, Chem. Mater. 12 (2000) 3715.
[16] A. Martínez-Arias, M. Fernández-García, O. Gálvez, J.M. Coronado, J.A. Anderson, J.C. Conesa, J. Soria, G. Munuera, J. Catal. 195 (2000) 207.
[17] D.-H. Tsai, T.-J. Huang, Appl. Catal. A 223 (2002) 1.
[18] A. Martínez-Arias, R. Cataluña, J.C. Conesa, J. Soria, J. Phys. Chem. B 102 (1998) 809.
[19] A. Martínez-Arias, M. Fernández-García, J. Soria, J.C. Conesa, J. Catal. 182 (1999) 367.
[20] P. Bera, S. Mitra, S. Sampath, M.S. Hegde, Chem. Commun. 927 (2001).
[21] J.B. Wang, D.-H. Tsai, T.-J. Huang, J. Catal. 208 (2002) 370.
[22] B. Skårman, L.R. Wallenberg, P.-O. Larsson, A. Andersson, J.-O. Bovin, S.N. Jacobsen, U. Helmersson, J. Catal. 181 (1999) 6.
[23] Y. Fu, Y. Tian, P. Lin, J. Catal. 132 (1991) 85.
[24] M. Fernández-García, A. Martínez-Arias, J.A. Anderson, J.C. Conesa, J. Soria, Stud. Surf. Sci. Catal. 130 (2000) 1325.
[25] A. Martínez-Arias, J. Soria, J.C. Conesa, X.L. Seoane, A. Arcoya, R. Cataluña, J. Chem. Soc. Faraday Trans. 91 (1995) 1679.
[26] A.B. Hungría, A. Iglesias-Juez, A. Martínez-Arias, M. Fernández-García, J.A. Anderson, J.C. Conesa, J. Soria, J. Catal. 206 (2002) 281.
[27] A. Martínez-Arias, M. Fernández-García, V. Ballesteros, L.N. Salamanca, J.C. Conesa, C. Otero, J. Soria, Langmuir 15 (1999) 4796.
[28] A. Martínez-Arias, M. Fernández-García, A. Iglesias-Juez, A.B. Hungría, J.A. Anderson, J.C. Conesa, J. Soria, Appl. Catal. B 38 (2002) 151.
[29] R. Hesse, T. Chassé, R. Szargan, Fresenius J. Anal. Chem. 365 (1999) 48.
[30] J.P. Holgado, R. Alvarez, G. Munuera, Appl. Surf. Sci. 161 (2000) 301.
[31] A. Martínez-Arias, M. Fernández-García, A. Iglesias-Juez, A.B. Hungría, J.A. Anderson, J.C. Conesa, J. Soria, Appl. Catal. B 31 (2001) 51.
[32] A.A. Davydov, in: C.H. Rochester (Ed.), Infrared Spectroscopy of Adsorbed Species on the Surface of Transition Metal Oxides, Wiley, New York, 1990, p. 75.
[33] A. Martínez-Arias, unpublished results.
[34] G. Ghiotti, F. Prinetto, Res. Chem. Intermed. 25 (1999) 131.
[35] P. Fornasiero, J. Kašpar, Collect. Czech. Chem. Commun. 66 (2001) 1287.
[36] K. Hadjiivanov, V. Avreyska, D. Kissurski, T. Marinova, Langmuir 18 (2002) 1619.
[37] A. Martínez-Arias, M. Fernández-García, A.B. Hungría, J.C. Conesa, G. Munuera, in preparation.
[38] C.D. Wagner, Faraday Discuss. Chem. Soc. 60 (1975) 291.
[39] G. Moretti, J. Electron. Spectrosc. Relat. Phenom. 95 (1998) 95.
[40] J.A. Mejias, V. Jiménez, G. Lassaletta, A. Fernández, J.P. Espinós, A.R. González-Elipe, J. Phys. Chem. 100 (1996) 16255.
[41] G. Moretti, Zeolites 14 (1994) 469.
[42] Y. Hu, L. Dong, M. Shen, D. Liu, J. Wang, W. Ding, Y. Chen, Appl. Catal. B 31 (2001) 61.
[43] P. Hollins, Surf. Sci. Rep. 16 (1992) 51.
[44] M.B. Padley, C.H. Rochester, G.J. Hutchings, F.J. King, J. Catal. 148 (1994) 438.
[45] A.A. Davydov, Kinet. Katal. 26 (1985) 157.
[46] A. Martínez-Arias, M. Fernández-García, C. Belver, J.C. Conesa, J. Soria, Catal. Lett. 65 (2000) 197.
[47] M. Fernández-García, I. Rodríguez-Ramos, P. Ferreira-Aparicio, A. Guerrero-Ruiz, J. Catal. 178 (1998) 253.
[48] S. Hoçevar, J. Batista, J. Levec, J. Catal. 184 (1999) 39.
[49] F. Mehran, S.E. Barnes, G.V. Chandrashekhar, T.R. McGuire, M.W. Shafer, Solid State Commun. 67 (1988) 1187.
[50] W. Daniell, N.C. Lloyd, C. Bailey, P.G. Harrison, J. Phys. IV France 7 (1997) C2–963.
[51] M. Fernández-García, E. Gómez Rebollo, A. Guerrero Ruiz, J.C. Conesa, J. Soria, J. Catal. 172 (1997) 146.
[52] F. Coloma, B. Bachiller-Baeza, C.H. Rochester, J.A. Anderson, Phys. Chem. Chem. Phys. 3 (2001) 4817.
[53] Y.A. Lokhov, V.A. Sadykov, S.F. Tikhov, V.V. Popovskii, Kinet. Katal. 26 (1985) 177.